A global model of the electromagnetic background noise

LISA ROSENQVIST, ELIN RABE

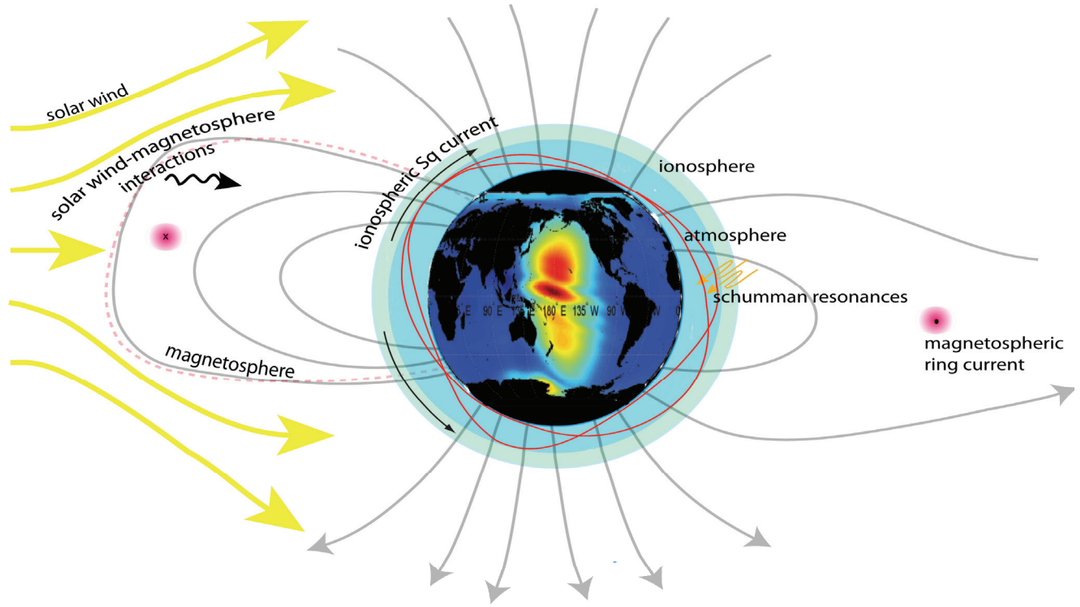

FOI
Defence Research Agency
Defence & Security,
Systems and Technology
SE-164 90 Stockholm

Phone: +46 8 555 030 00
Fax: +46 8 555 031 00

www.foi.se

FOI-R--3236--SE Scientifc report
ISSN 1650-1942 September 2011

Defence & Security, Systems and Technology

Lisa Rosenqvist, Elin Rabe

A global model of the electromagnetic background noise

Cover illustration: Schematic illustration of the physical processes that contribute to the electromagnetic background noise. The global color map represents the magnetospheric and ionospheric field variation at the surface of the Earth as computed with the CM4 model.

Titel	Modellering av den elektromagnetiska brusbakgrunden
Title	A global model of the electromagnetic background noise
Rapportnummer / Report no	FOI-R--3236--SE
Rapporttyp / Report type	Scientific report / Vetenskaplig rapport
Månad / Month	September
Utgivningsår / Year	2011
Antal sidor / Pages	30
ISSN	ISSN-1650-1942
Kund / Customer	FOI
Projektnummer / Project no	E20684
Godkänd av / Approved by	Nils Olsson Head, Defence & Security, Systems and Technology

FOI Swedish Defence Research Agency
Defence & Security, Systems and Technology
SE-164 90 STOCKHOLM

Abstract

We present the recent development of an empirical global model of the electromagnetic background noise. The model takes into account the main contribution from this background field originating from the Earth space environment. The model is developed on the basis of a global geomagnetic field model to find the spatial and temporal variation of the near DC magnetic disturbance across the globe. The extension of this DC level to the full geomagnetic spectrum (up to 10 Hz) is obtained by investigating the statistical behavior of the magnetic spectrum based on experimental data. It is found that the spectrum can be modeled with power laws with exponents linearly dependent on the level of geomagnetic activity, i.e. on the KP index. This linear dependence is in turn a function of latitude and time. The modeled magnetic spectrum as well as knowledge of the electrical conductivity profile in the Earth's crust further permits determination of the electric wave power spectrum with depth.
Finally, the model is validated by comparison with experimental electromagnetic data from FOI's test site in the Stockholm archipelago where environmental parameters are known from previous field trials. The model gives excellent results in the higher frequency domain (0.1-10 Hz) while for lower frequencies one must probably account for contributions from ocean circulation.
The ability to predict the electromagnetic background noise is important for both civilian, e.g. geophysical and aeromagnetic survey planning, as well as military applications, e.g. to evaluate protection, security and capability of naval systems with the use of tactical decision aids.

Keywords

Electromagnetic noise, geomagnetic activity, tactical decision aids, detection probabilites, sensors

Sammanfattning

Vi presenterar den senaste utvecklingen av en empirisk global modell av det elektromagnetiska bakgrundsbruset. Modellen tar hänsyn till det dominerande bidraget till det elektromagnetiska bakgrundsbruset som har sitt ursprung från jordens närrymdmiljö. Modellen är utvecklad utifrån en global modell över variationerna i det jordmagnetiska fältet för att uppskatte nivån av magnetiska störningar nära DC som funktion av rum och tid. Denna DC nivå relateras sedan till hela jordmagnetiska spektrumet (upp till 10 Hz) genom att undersöka statistiska egenskaper av det magnetiska spektrumet baserat på experimentella data. Experimentalla data visar att spektrumet kan modelleras med potenslagar vars exponenter är linjärt beroende av geomagnetiskt aktivitet, kvantifierat genom det så kallade KP indexet. Detta linjära beroende är i sin tur en funktion av latitud och tid. Det modellerade magnetiska spektrumet samt kunskap om vertikala variationer i jordskorpans elektriska ledningsförmåga möjliggör ytterligare bestämning av det elektriska spektrumet som funktion av djup.
Slutligen valideras modellen genom jämförelse med experimentella elektromagnetiska data från FOI:s provplats i Stockholms skärgård där miljöparametrar är kända från tidigare fältförsök. Modellen ger goda resultat i högre frekvens domän (0.1-10 Hz) medan man för lägre frekvenser troligtvis måste ta hänsyn till bidrag från havsströmmarna.
Förmågan att förutse det elektromagnetiska bakgrundsbruset är viktigt för både civila tillämpningar, t.ex. inför planering av geofysiska och magnetiska undersökningar, såväl som militära tillämpningar, t.ex. utvärdera skydd, säkerhet och förmåga hos marina system med taktiska stödsystem.

Nyckelord

Elektromagnetiskt brus, geomagnetisk aktivitet, taktiska stödsystem, detektionssannolikhet, sensorer

Contents

1 Introduction **7**

2 Method **9**

3 Global EM model **11**

3.1 Geomagnetic noise 11

3.1.1 Global geomagnetic field model 11

3.1.2 Geomagnetic spectrum 11

3.2 Geoelectric noise 19

4 Model validation **23**

5 Conclusions **25**

Bibliography **29**

1 Introduction

Earth is continuously exposed to electromagnetic (EM) radiation which sets up a natural background EM noise floor. There are a number of emissions that contribute to the ambient EM noise. Close to urban areas man-made sources from e.g. cables, railways, pipelines or power lines can make up a large part of the EM noise background. For underwater applications it is also important to take the sources from the ocean itself into account, such as EM noise generated via waves and currents. The most dominant source of the EM-fields, however, originates from the high atmosphere and interactions between the space environment and the solar wind.

Diurnal solar heating of the ionized part of the high atmosphere, the ionosphere, cause convective motion of charged particles across the geomagnetic field at middle and low latitudes. This induce electric fields and currents at approximately 100 km altitude, which produce a regular and broad-scale daily variation of the geomagnetic field. Apart from this *solar quiet* daily variation there are other fluctuations associated with geomagnetic disturbances related to solar activity. The timescales of these variations vary from hours (geomagnetic substorms) to several days (geomagnetic storms) and occur irregularly but more frequently during the active years of the 11-year solar cycle. Direct modulation of the solar wind by Earth's protective magnetic cavity, the magnetosphere, also generate micropulsations in the frequency band 0.002-0.2 Hz. These oscillations are categorized as Pulsation continuous (Pc) and divided into five classes of specific frequency bands and are most frequent during daytime. At local night time, oscillations are more irregular and generally have the appearance of transients (pulsation irregular). Another geoelectric phenomenon that contributes to the EM noise floor is the Schumann resonances. These oscillations are global EM resonances, excited by global lightning activity in the cavity formed by the Earth's surface and the ionosphere which acts as a closed waveguide. Schumann resonaces are the principal background in the electromagnetic noise spectrum distributed in distinct peaks between 3 to 60 Hz (first Schumann resonance at 7.8 Hz). A composite amplitude spectrum of geomagnetic field variations as a function of frequency is given in Constable & Constable (2004) and an schematic illustration of the physical processes that contribute to the electromagnetic background noise is given in Figure 1.1. The color map represents the magnetospheric and ionospheric field variation at the surface of the Earth as computed with a global geomagnetic field model that have been throughout this study. As the externally generated EM fields propagate through a medium they are modified through the material properties by the very medium of propagation. Thus, to be able to predict the EM background noise floor for a given location and at a given depth it is necessary not only to have a good estimate from all the EM field sources mentioned above but also to have a good knowledge of the surrounding environmental conditions. For example, sediment stratification and sedimentary properties such as electrical conductivity and permittivity.

The ability to predict this natural EM noise floor is important for a wide range of applications. Forecasting tools of geomagnetic pulsations could be useful in the planning of aeromagnetic surveys Vallee *et al.* (2005) as well as in the design phase of EM geophysical surveys. From a space weather perspective 1-10 mHz ultra-low frequency wave power are strongly correlated with e.g. solar wind speed, geomagnetic activity, and relativistic electron flux in the magnetosphere and the prediction of the wave power could thus be used as an

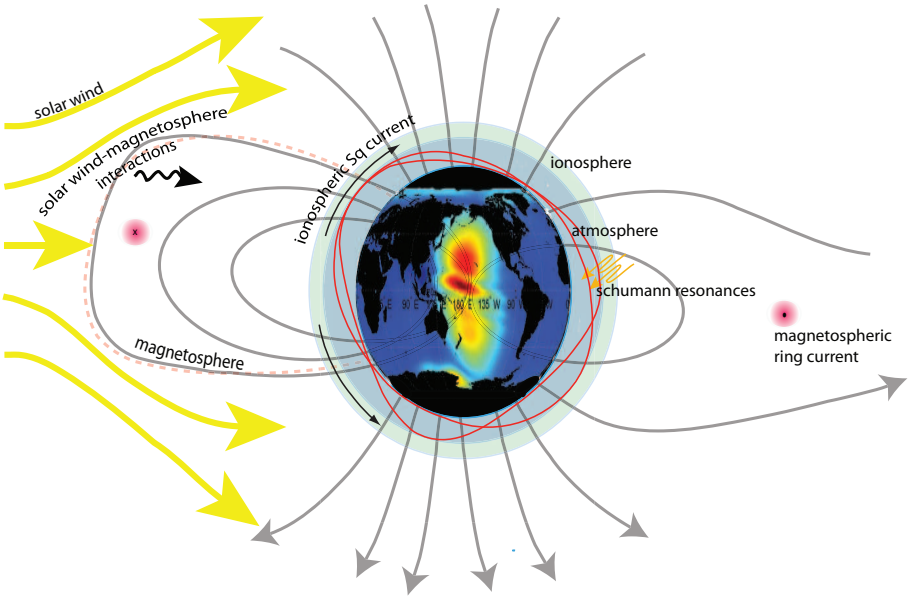

Figure 1.1: Scematic llustration of the physical processes behind the electromagnetic background noise.

effective proxy of such parameters (e.g. Mann *et al.* (2004)). For military purposes the knowledge of the full properties of the EM background noise are connected to a range of activities from mine warfare to detection probabilities, ranges, and sensor capability for different underwater systems.

The aim of this model is not to develop a detailed and precise prediction of the global EM wave power but rather to develop a model that can give an approximate level of the EM background noise floor at a given frequency (from near DC to 10 Hz) to be used as a reference level in military tactical support systems.

Outline

The remainder of this report is organized as follows. Section 2 describes the proposed method to develop the global electromagnetic model of the natural background noise. In section 3 we study the geomagnetic spectra based on observations combined with a model of the geomagnetic field. Further we transform the geomagnetic spectra into a geoelectric spectra based on the theory of electromagnetic induction in the Earth. The model is validated by comparisons with real observations in Section 4. Finally, Section 5 gives the conclusions.

2 Method

In this section we aim at describing the method used to model the global EM background noise originating from variations in the geomagnetic field described in the introduction. At this point we do not intend to include any other sources, such as anthropogenic or ocean contributions, although this could be considered in a future development of the model. Our method to develop the model is composed of the following three steps:

Step 1: The external EM field varies with both time and geographic position. As the development of a global model of this variation across the full spectral band of interest is a demanding task we intend to make use of previous efforts to model the global geomagnetic field. We will use one such existing model to estimate the daily wave power amplitude, i.e. at a 24 hour period.

Step 2: As many of the applications are dependent upon knowledge of the EM noise floor at a range of frequencies it is necessary to relate this daily wave power amplitude (near DC level) to the full geomagnetic spectrum. In this step we use available geomagnetic data to study the statistical properties of the geomagnetic spectrum and relate these to the daily level acquired in the first step. However, this study is limited to model the spectrum to an upper frequency of 10 Hz. This limitation is a consequence of the use of data with a sampling rate of 1-40 Hz.

Step 3: Lastly, to develop a complete electromagnetic model of the background noise we need to relate the obtained geomagnetic spectra to the geoelectric spectra. Knowledge of the electrical conductivity profile in the Earth's crust and the theory of electromagnetic induction in the Earth further permits determination of the vertical electric wave power spectrum.

Figure 2.1 illustrates the three method steps. The first panel shows the global modeled magnetospheric and ionospheric magnetic field on the Earth surface at 00 UT the 1st of Mars, 2007. The middle panel shows the daily magnetic spectra recorded with instruments from the Swedish Defence Research Agency's (FOI) test site Djupviken and from Fiby, Uppsala, compared to the modeled spectra from for the same day. And the last panel illustrates an electromagnetic plane wave, incidenting vertically, exciting the Earth consisting of plane homogeneous layers.

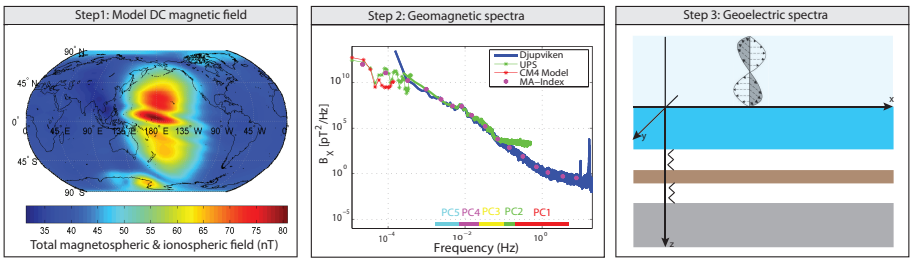

Figure 2.1: Illustration of the three steps in the method to develop the model of the global geo-electromagnetic background noise.

3 Global EM model

In this section we describe the development of the noise model according to the method described in the previous section.

3.1 Geomagnetic noise

3.1.1 Global geomagnetic field model

There are several existing models of the global geomagnetic field, however, the Comprehensive Modeling (CM4) of the geomagnetic field models all sources that contribute to the geomagnetic field Sabaka *et al.* (2004). It accounts for the fields originating from the Earth core, the crustal field of lithospheric origin, as well as the magnetospheric and ionospheric fields. The two latter are the important contributions for this work as the core and crustal fields vary on secular and geologic timescales. CM4 is derived from hourly average magnetic data from observatories and satellites. Thus, it can be used to give the daily wave power amplitude, i.e. at a 24 hour period, as a function of time, location, and solar activity in the form of the Disturbance storm time (Dst) index and F10.7 solar radio flux. These activity indices can be downloaded from the Coordinated Data Analysis Web (CDAWeb) and be used as input to CM4.

Figure 3.1 is a comparison of the horizontal component ($B_T = \sqrt{B_x^2 + B_y^2}$) of the magnetic field modeled with CM4 and measurements from the magnetic station in Uppsala (UPS) which is an INTERMAGNET Magnetic Observatory (IMO) for the month of March, 2007. The observed magnetic field from UPS are shown as the black line in Figure 3.1 and the diurnal solar quiet variation is clearly seen. The core field modeled by CM4 is shown as the green line in Figure 3.1. As this accounts for about 97-99 percent of the total field we have normalized the values with the mean of the variation to be able to see it on the same scale. Further, we have added the different magnetic field contributions to the core field modeled by the CM4 model, the crustal field (pink line), the magnetospheric field (blue line) and the ionospheric field (red line). It is evident that as we add the different contributions the prediction of the field variation become increasingly accurate. CM4 is derived from hourly averages and thus cannot resolve finer scale variations. Moreover, it is derived for magnetospheric quiet periods which mean that it cannot account for magnetically disturbed periods. During the periods where rather large deviations between the data and the model are seen (e.g. 5-9 March) the level of geomagnetic disturbance quantified by the official planetary KP-index was high.

3.1.2 Geomagnetic spectrum

3.1.2.1 Linear Regression Model

The CM4 model can only give us the magnetic wave power at periods between 2 and 24 hours. As we are interested in much higher frequencies we need to investigate how we can extrapolate the spectrum up to 10 Hz from the magnetic wave power level derived from CM4. Thus, we have investigated statistical properties of the geomagnetic wave power spectrum from experimental data. The lower frequency end of the spectra is derived from 3-axis magnetic field

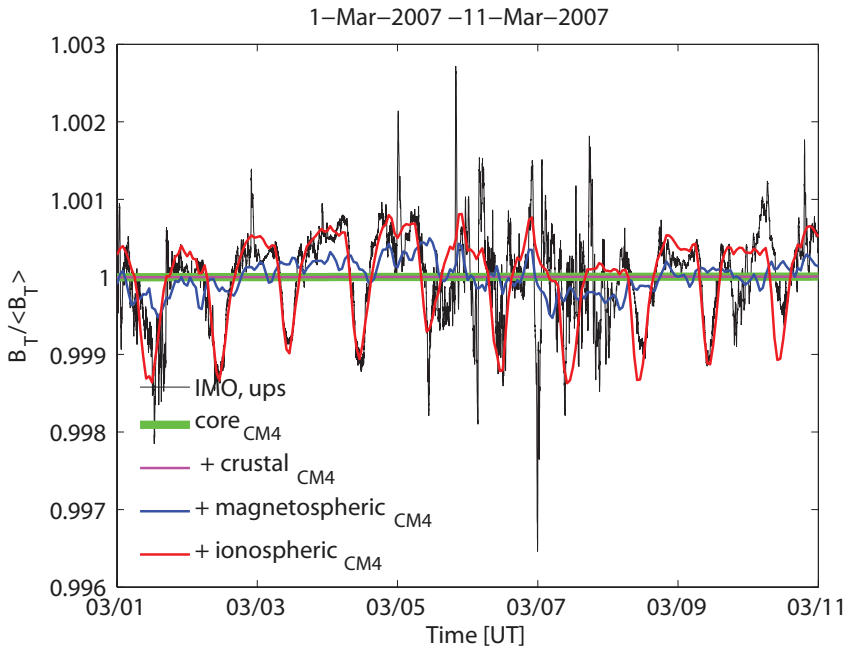

Figure 3.1: Comparison of the CM4 model with IMO UPS data.

fluxgate data sampled at 1 Hz from IMO/UPS. To account for magnetic field variations at higher frequencies we have superimposed data from FOIs own 2-axis magnetic field induction coil data sampled at 40 Hz from Djupviken south of Stockholm. The data cover four consecutive months, from 1st of March to 1st of June in 2007. Prior to processing, days with unreliable data were removed from the dataset resulting in a total of 93 days to be investigated.

The calculation of the power spectra consisted of using a conventional Fourier transform. For this purpose, we used 24 hour time intervals weighted by a Hanning window. Prior to this the induction coil data was high pass filtered at $5 \cdot 10^{-5}$ Hz. Further we define the Magnetic Activity (MA) index as the 16 average spectral estimates calculated in $\mathrm{pT}^2/\mathrm{Hz}$ in different frequency bands in accordance to the analysis of magnetic data from the Northern California Earthquake Data Center (NCEDC) by Dr. Martin Fullekrug at the University of Bath. The frequency bands for the 16 MA indices are shown in Table 3.1.

Figure 3.2 shows the daily magnetic spectra for 1st of March 2007 from Djupviken (blue line), from UPS (green line) and from CM4 (red line) together with the 16 MA-indices estimates (pink dots). Also indicated in the figure are the frequency bands covered by the five classes of Pc micropulsations (Pc1-5).

One way to study the behavior of the geomagnetic spectra is by applying linear regression to the daily MA indices in a least squares sense and investigate the temporal evolution of the spectral slope. The goal would be the ability to parameterize this slope with the value from CM4 at T=24 hours and possible other predictable parameters. As geomagnetic variations are strongly related to geomagnetic activity it seems natural to investigate the possibility to parameterize the slope with the KP index. After investigating the variation of the spectral slope during the 93 days of data we suggest a predictive simple model of the geomagnetic spectra according to Figure 3.3. The geomagnetic spectra in the frequency range 10^{-5} to 10 Hz is divided into three regions were the following models are applied:

Table 3.1: MA Magnetic Activity Indices

Index	Period (s)	Frequency (Hz)
MA1	25000-83000	0.000012-0.00004
MA2	5300-25000	0.00004-0.00019
MA3	1800-5300	0.00019-0.00056
MA4	600-1800	0.00056-0.0017
MA5	300-600	0.0017-0.0033
MA6	150-300	0.0033-0.0067
MA7	100-150	0.0067-0.01
MA8	45-100	0.01-0.022]
MA9	20-45	0.022-0.05
MA10	10-20	0.05-0.1
MA11	5-10	0.1-0.2
MA12	2-5	0.2-0.5
MA13	1-2	0.5-1
MA14	0.5-1	1-2
MA15	0-17-0.5	2-6
MA16	0.1-0.17	6-10

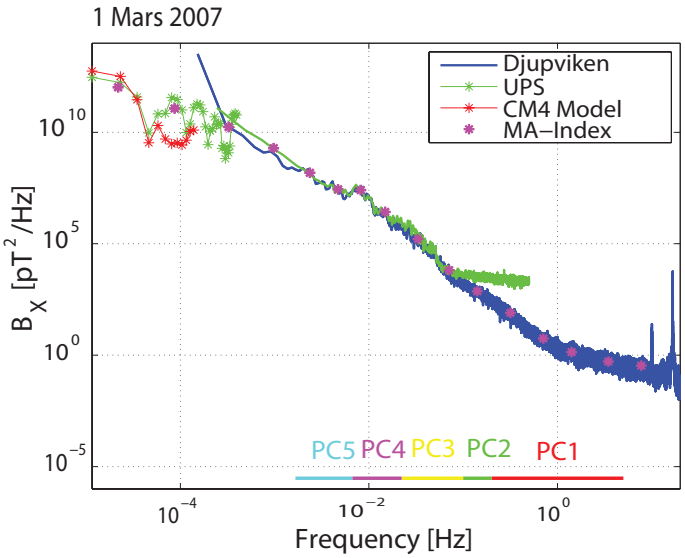

Figure 3.2: Geomagnetic spectra for 1 Mars 2007 based on UPS fluxgate data (green line), Djupviken induction coil data (blir line) and as estimated from the CM4 model (red line). The MA indices are shown as pink dots and the different frequency ranges of the Pc pulsations are indicated in the figure.

Region 1: A linear relation of the logarithms of the wave power and the frequency (power law):

$$\mathrm{MA}(F)_1 = k_1 F + m_1, \quad F = \log(f), \quad 10^{-5} < f \leq 10^{-3}\mathrm{Hz}. \tag{3.1}$$

Region 2: A linear relation of the logarithms of the wave power and the frequency (power law):

$$\mathrm{MA}(F)_2 = k_2 F + m_2, \quad F = \log(f), \quad 10^{-3} < f \leq 3\mathrm{Hz}. \tag{3.2}$$

Region 3: Constant above $f > 3$ Hz.

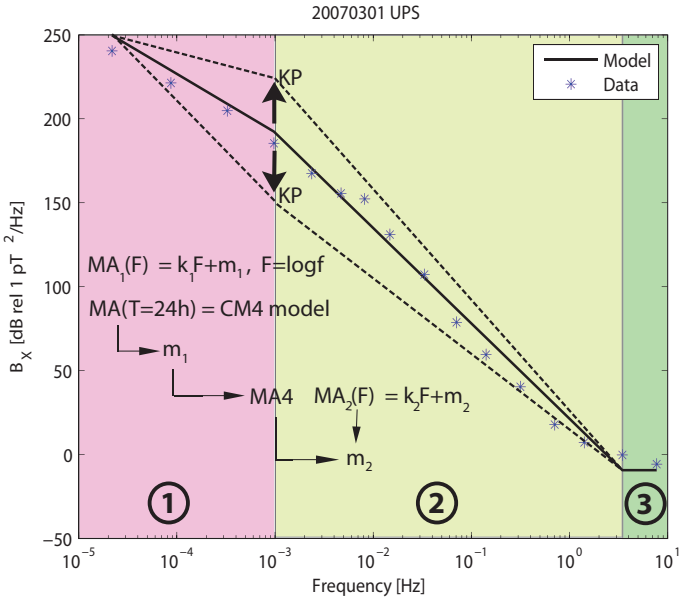

Figure 3.3: Approach for modeling the geomagnetic spectra.

3.1.2.2 Dependence on geomagnetic activity, KP

The reason to divide the spectra into these three regions is based on the finding that the spectral slope of the lower frequency part (Region 1) flattens with increasing geomagnetic activity (KP) while the spectral slope of the higher frequency region (Region 2) steepens with increasing KP. This finding is illustrated in Figure 3.4. In the first panel the best-fit spectral slope for region one is shown as blue dots for the entire dataset (93 points) and the best-fit spectral slope for region two are shown in blue dots as a function of KP[1]. The linear regression model (LRM) parameterized by KP is shown with the respective solid lines. It is clear that the two LRMs for the two regions have slopes with opposite signs. The correlation coefficient of the spectral slope and KP for both regions are high, R=0.78 and R =0.84, respectively. This high correlation results in a relatively accurate model of the temporal evolution of the spectral slope in the different regions shown in the left panel of Figure 3.4. The modeled slope is shown with the red lines and the best-fit slopes are illustrated with blue and green for region one and two respectively. Thus, we can model the spectral slopes of the different regions as

$$k_i(t, \varphi, \mathrm{KP}) = a_i(t, \varphi)\mathrm{KP} + b_i(t, \varphi), \quad i = 1, 2 \tag{3.3}$$

where the LRM parameters a_i and b_i are functions of latitude (φ) and time (t) as one can expect a solar cycle dependence.

3.1.2.3 Latitudinal dependence of region one

To find the dependence on the LRM parameters for region one with latitude we make use of the extensive IMO database. A large number of IMO stations are spread throughout the world from Hornsund on Svalbard at a latitude 77°N to Scott Base in Antarctica at 78°S. One minute mean data, corrected for spikes,

[1]Three hour KP index for this period has been downloaded from the Coordinated Data Analysis Web (CDAWeb).

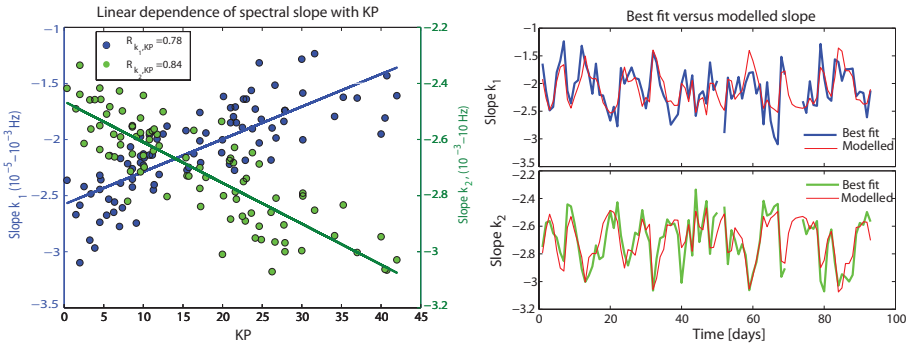

Figure 3.4: The linear dependence of the spectral slopes in the two different regions with KP for the Uppsala/Djupviken dataset.

gaps and baseline variations, are freely available on the INTERMAGNET website. Magnetic field data for the north component (B_x) and the east component (B_y) for a selected number of stations (34 st) spread in the latitude band $\pm 70°$ have been analyzed for all of 2007. The linear dependence of the spectral slope of the first region (limited by the one minute mean sampling) with KP for the north and east components have been investigated for all stations during 2007. The resulting latitudinal dependence of the LRM parameters a_i and b_i are shown in Figure 3.5. In the top panel the slope of the LRM for the north (a_1^x) and east (a_1^y) component is shown with green circles and red squares respectively. A best fit 7th order polynomial of the points is shown as the green and red solid lines. An identical representation for the intercept (b_1^x and b_1^y) of the LRM is shown in the bottom panel. It would also be possible to find the dependence on the LRM parameters for region one with time by performing the same analysis for several consecutive years. However, this will be investigated in future work on this model.

3.1.2.4 Temporal and latitudinal dependence of region two

To investigate the latitudinal dependence of the LRM parameters of region two proves to be a little more difficult as data at the required sampling rate (at least 40 Hz) is not as easily acquired. However, we have already found the parameters for the four month period of Uppsala data, i.e. at a latitude of about 60°N (see Figure 3.4). Moreover, MA index data are available from the NCEDC website from two stations in California, Parkfield (PKD) and Hollister (SAO) at a latitude of about 36°N. This database covers a total of nine years ranging from 1996 to 2004 and constitute thirteen average MA indices (MA4-16) spaced by 15 minute intervals. However, these stations are subject to electromagnetic noise due to the San Francisco Bay Area Rapid Transit (BART) DC electric railway and thus long periods of the database are infected with large spikes and disturbances (Egbert *et al.* (2000)). Although, comparisons of the data from the two stations show that PKD is least influenced by BART as a natural consequence of the longer distance from this station to San Francisco. Thus, we have analyzed data from PKD only. Periods of large spikes and strong disturbances have simple been removed from the dataset prior to the analyze.

The 15 minute mean MA indices have been recalculated to daily average MA indices and the LRM parameters for region two , a_2 and b_2, have been calculated

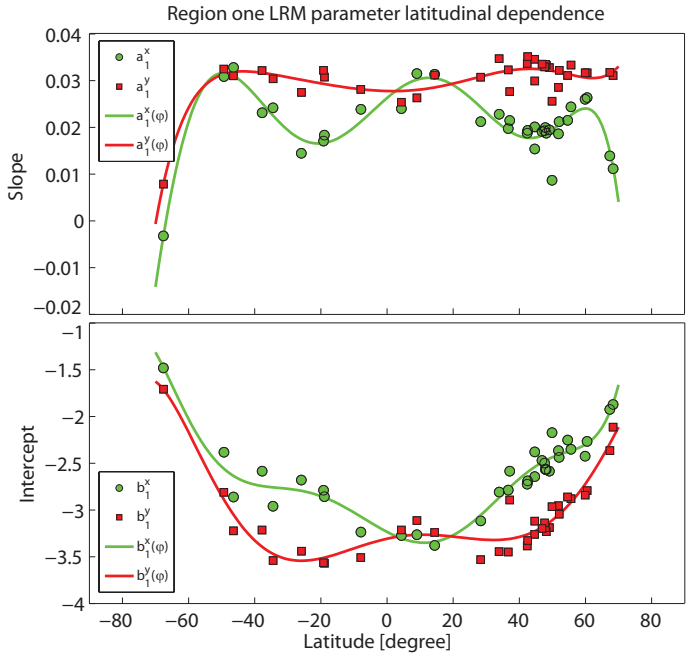

Figure 3.5: The latitudinal dependence of the LRM parameters of the spectral slope of region one derived from data for all of 2007 from 34 IMO stations spread across a latitudinal band of $\pm 70^{\circ}$.

for the nine years of PKD data and is shown in Figure 3.6. The figure layout is identical to Figure 3.5 with the top panel showing the slope of the LRM for the north (a_2^x) and east (a_2^y) component is shown with green circles and red squares respectively while the middle panel shows the intercept (b_2^x and b_2^y). The bottom panel shows the yearly mean KP index from 1996 until 2009. The temporal evolution of the LRM parameters seem to be linearly proportional to the yearly mean KP index as shown by the fitted green and red lines through the points. This could be expected as the spectral slope is dependent on KP index and thus the yearly LRM parameters of this slope could be expected to depend on the yearly level of activity, i.e. follow the 11-year solar activity cycle. However, there is a discrepancy for the first three years 1996-1998. The reason for this is not clear but it might be related to the identification of very large activity in the Pc1 frequency band at PKD during these years. Weather this high activity is a consequence of natural or artificial disturbances is not clear. Superimposed on the PKD parameter in Figure 3.6 are the results from the investigated 4 months of UPS data (shown with the cyan dots and squares for the x and y-component respectively). As there are no PKD data available for 2007 a direct comparison is not possible, however, the LRM parameters from UPS agree rather well with the predicted PKD LRM parameters parametrizised by the yearly mean KP. Thus, in the lack of available high resolution data from other latitudes that prevents the study of the latitudinal dependence of the LRM parameters from region two we assume that the LRM parameters are constant with latitude and only exhibit a temporal behavior. This is a very strong assumption based on investigations from merely two different latitudes and should naturally be studied more extensively in a future study.

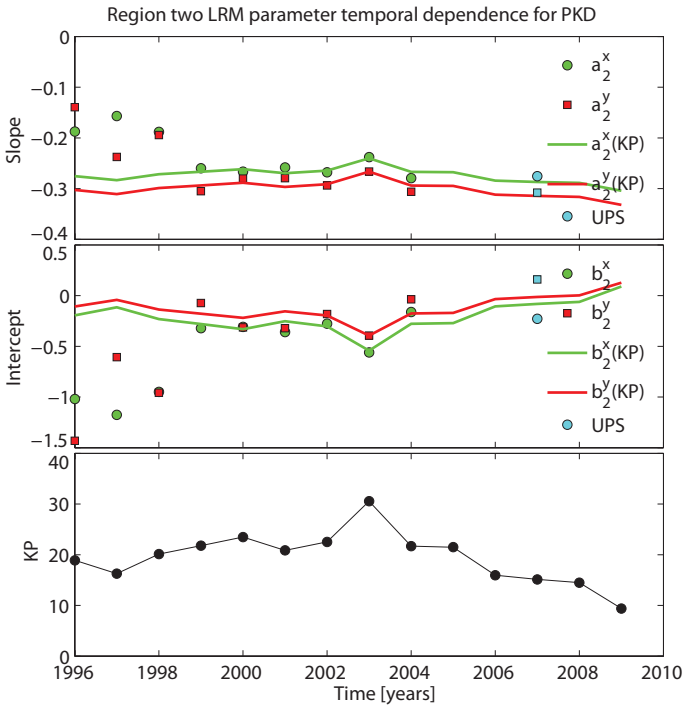

Figure 3.6: The temporal dependence of the LRM parameters of the spectral slope of region two derived from PKD data (36°N) during the years from 1996 to 2004. Superimposed are the LRM parameters derived from UPS data (60°N) during four months of 2007.

3.1.2.5 Validation of geomagnetic spectral model

To investigate how well the geomagnetic spectral model outlined above can represent observations we have compared the model output to the 93 days of magnetic observations from Uppsala and Djupviken. The magnetic spectra of the x and y-component is shown in the upper panels of Figure 3.7. The blue lines in the lower panels show the range of the observations at each frequency (i.e. the distance between the thicker black lines in the upper panel) together with the mean error and standard deviation between the model and the observations for all 93 days. The mean model error for the latitude of Uppsala does not exceed 10 dB across the frequency range and is consistently lower than the range of the data except from the point where the data range is minimum.

Next we investigate the accuracy of the geomagnetic spectral model for the year of 2007 which is shown in Figure 3.8 for the x-component (left figure) and y-component (right figure) respectively. It shows the absolute error in dB between the observed spectra and the modeled spectra in colorcoding for the investigated latitudes and in the different frequency bands. It should be noted that the y-axis is not linear in latitude. Furthermore, we have not analyzed data for PKD during 2007, thus the error for PKD in Figure 3.8 is based on data from 1999. The year of 1999 was chosen to represent a similar period of the solar cycle as 2007, however, excluding the years from 1996-1998 when there is a unknown discrepancy in the LRM parameters from a solar cycle dependence (see Figure 3.6). The mean error during 2007 for the x-component is between 5-10 dB for most latitudes and frequency bands. However, there are a few exceptions. First, stations at high latitudes have higher mean errors.

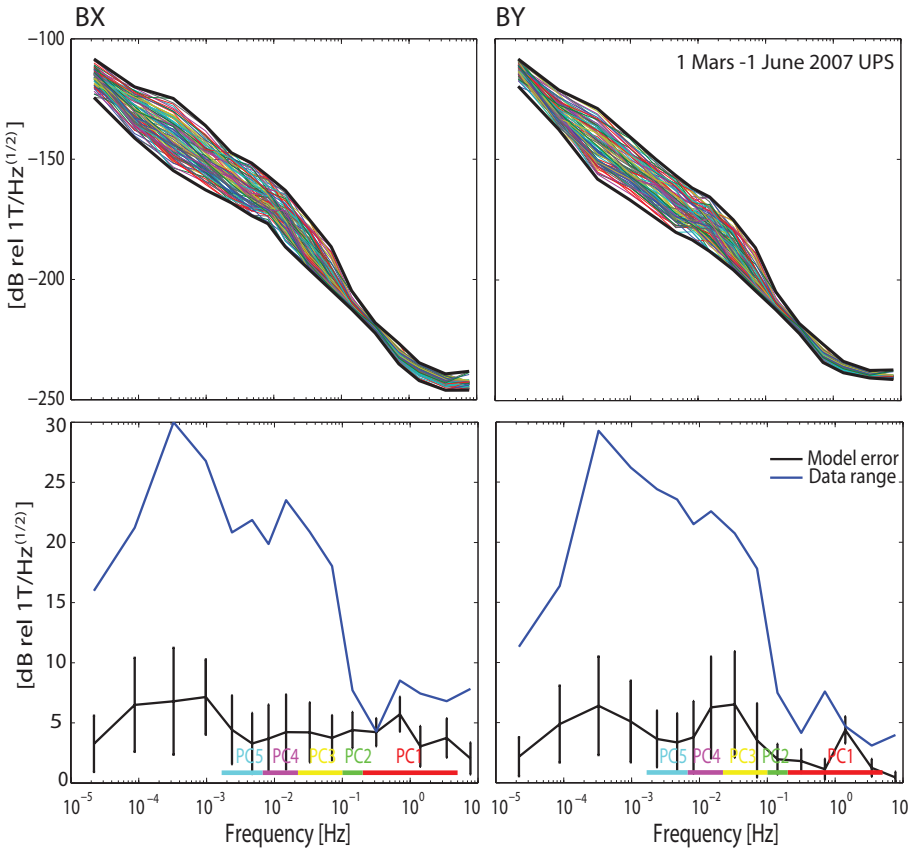

Figure 3.7: The upper two panels show the magnetic spectra for 93 days in Uppsala x-component (to the left) and y-component (to the right) respectively. The lower panel shows the range of the data in the upper panel (blue line) and the mean error and standard deviation between model and observations in the black line. The different frequency ranges of the Pc pulsations are indicated in the figure.

This is due to their location close to the auroral oval, a geomagnetically very active region. As the CM4 model is derived from geomagnetically quiet periods it cannot accurately model the base value at these latitudes and thus the power of the modeled spectra is far too low. Another region where the error increases rather dramatically is in the 0.1-1 Hz frequency band for PKD at a latitude of 35.9°N. The reason for this is the departure from a power law in the second region of the geomagnetic spectra. The spectra must be modeled with at least a polynomial to accurately represent the data. This might be due to a band-limited enhancement in the Pc3-4 spectra observed in PKD as well which has also been identified at other locations (Ponomarenko *et al.* (2002)). However, there is also evidence of a superimposed effect from excitation of electromagnetic noise from BART on these natural enhancements and the relative contribution from these two sources is still not clear (Egbert *et al.* (2000)).

Also, it can be noted that there is an north/south asymmetry in the mean error for the y-component with larger errors for northern latitudes (between 40°N and 60°N). The reason for this discrepancy is due to a seasonal and latitudinal discrepancy between the modeled MA1 index for the y-component from CM4 and the real observed value for the IMO stations. During the winter months for northern latitudes the CM4 model deviates substantially from the

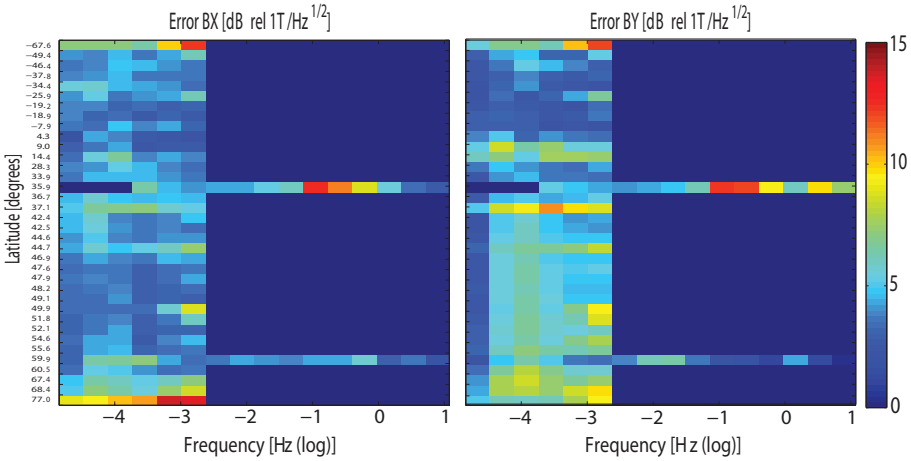

Figure 3.8: The absolute error in dB between observed and modeled geomagnetic spectra as a function of latitude and frequency.

observations for the y-component (see Figure 3.9). As the whole approach of modeling the geomagnetic spectra is based on an accurate estimation of the MA1 index the errors remain large throughout the entire frequency band for the y-component at these latitudes. However, the errors are only enhanced during the winter months, January, February and December but do influence the calculated mean error in Figure 3.8.

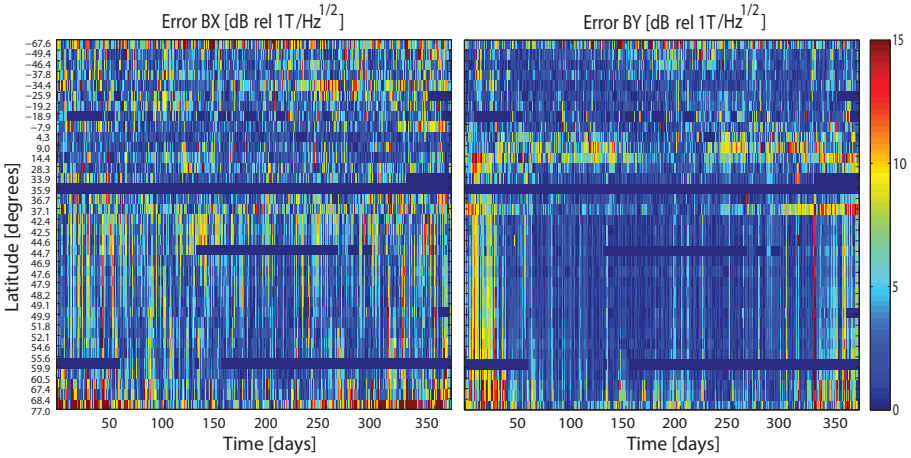

Figure 3.9: The absolute error in dB between observed and modeled MA1 index (from CM4) as a function of latitude and days in 2007.

3.2 Geoelectric noise

To further estimate the electrical noise level at the surface and/or at a given depth below the surface, a model is required to relate the magnetic signal to the electric. As the distance to the electromagnetic transmitter is large it is possible to consider the electromagnetic wave as plane and the magnetic and electric wave is perpendicular to both each other and the direction of propagation. Since the natural electromagnetic background has its origin in space far above the earth's surface, it is a reasonable assumption to regard the

waves as planar for this case. The natural variations in Earth's magnetic field induce electric fields and currents in the Earth's conductive materials. In the simplest case, one can assume that the Earth is composed of flat, homogeneous layers of material, such as water, sediment or rock. With knowledge of the bearing electrical conductivity, it is in this case a simple relation between the electric, and magnetic field, in the form of

$$E_{x,y} = \pm \underbrace{\frac{ik}{(\sigma - i\omega\epsilon)}}_{Z} H_{y,x} \tag{3.4}$$

for an upward wave where Z is the wave impedance. For an downward wave, the signs are reversed. Such a plane layered model of the earth consisting of N layers is illustrated in Figure 3.10 with a vertically incident plane electromagnetic wave. As the field components at the interfaces of the layers are

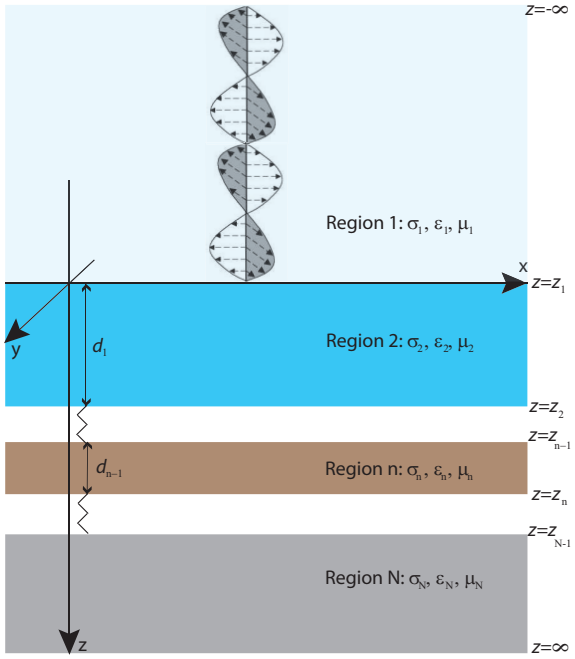

Figure 3.10: Illustration of a plane layered model of Earth with a vertically incident plane wave on the surface.

continuous, equation 3.4 can be used to determine the electrical noise level of an arbitrary depth, given that you have knowledge of the magnetic noise level and the underlying geological conductivity distribution (e.g. Berdichevsky & Zhdanov (1984)).

A first approximation of the underlying global conductivity distribution can be estimated from the 1° x 1° global sediment thickness map compiled by Laske & Masters (1997) (see figure 3.11 for the global topography) and have been derived by Everett *et al.* (2003). This map contains sediment density discretized in up to three layers, a surface layer up to 2 km thick, an underlying layer up to 5 km thick, and, where necessary, a third layer to make up total sediment thickness, which often exceeds 10 km. To estimate the conductivity in the different layers the world was divided into three regions based on topography;

1. the ocean basins and continental shelves defined by elevations below sea level,

2. the coastal plains and low-lying continental sedimentary basins defined by elevations above sea level but below 100 m, and

3. the continental interiors and highlands above 100 m elevation.

In region (1), the oceans, the ocean layer was assigned a conductivity of 3.2 S/m, the upper two sediment layers (up to 7 km thick) were assigned a conductivity of 0.8 S/m, and the deepest sediments assigned a conductivity of 0.02 S/m. In region (2), the coastal plains and low basins, the entire sedimentary section was assigned a conductivity of 0.5 S/m. In region (3), the continental highlands, the entire sedimentary section was assigned a conductivity of 0.03 S/m. The balance of the section to a depth of 50 km, representing oceanic and continental igneous rocks, was assigned a conductivity of 0.001 S/m. As the conductivity in the world oceans vary greatly (for example the conductivity in the Baltic sea is around 0.8 S/m) this model is indeed rather crude and can only provide a first approximate representation of the vertical conductivity distribution. We will further investigate the accuracy of using this crude model in the next section.

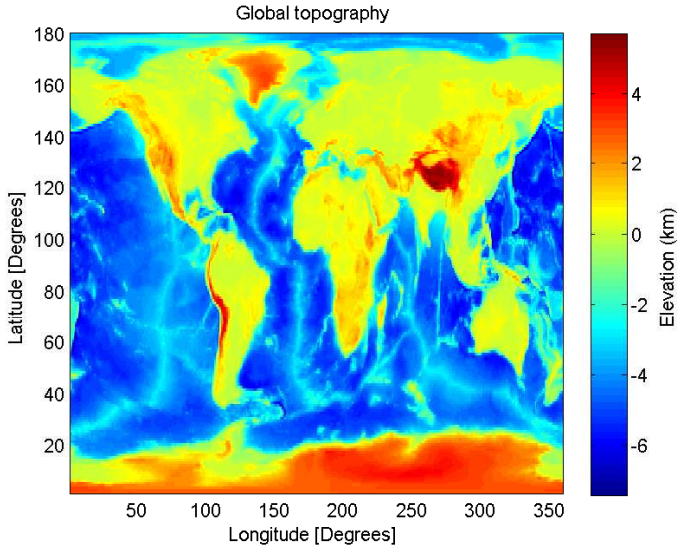

Figure 3.11: The global elevation based on the 1° x 1° sediment map by Lake and Masters Laske & Masters (1997).

4 Model validation

To validate the electric part of the global model of the geo-electromagnetic background noise we have compared the model results with experimental EM data from FOI's sea research site Djupviken that is part of the Horsfjärden bay in the Stockholm archipelago. The site is provided with 3-axis magnetic field induction coil instruments sampled at 40 Hz for continuous EM monitoring of the magnetic background. These data can be complemented by fluxgate magnetic field measurements sampled at 1 Hz from the Geological Survey of Sweden (SGU) in Uppsala some tens of kilometers away. Furthermore, two electrode sensor systems measuring the horizontal electric field components are placed at two separate locations off-shore for monitoring of the underwater electric environment. The north and south systems are situated at different depths, about 40 and 25 meters respectively. The topography of the Djupviken site is shown in Figure 4.1 as well as the locations of the two electrode sensor systems, north and south. As the underlying geology at this site has already been investigated in previous field trials it is an ideal test site to investigate the robustness of the induction model. We employed a four-layer model consisting of air, water with a conductivity of 0.8 S/m, a five-meter deep sediment layer with a conductivity of 0.5 S/m and bedrock with conductivity 0.005 S/m.

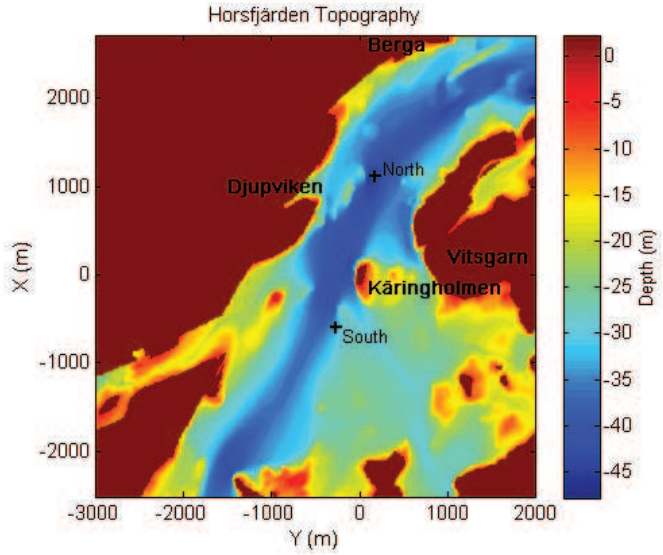

Figure 4.1: The bathymetry of the sea outside FOI's sea trial site in the Stockholm archipelago and the location of the north and south electric sensor systems respectively.

The results are displayed in Figure 4.2 for the electric x and y-component respectively. The blue dotted line represents the observed electric wave power at 25 meters depth while the red solid line represents the modeled electric wave power based on the observed magnetic spectra and the four-layer conductivity profile. The agreement between the two curves is high for the higher frequencies while they start to deviate for lower frequencies. Effects from ocean circulation or coastal effects might become important here (e.g. Tyler *et al.* (1997)). For comparison the red dashed line represents the modeled wave power based

on the modeled magnetic spectra and the four-layer conductivity profile and the red dotted line represents the modeled wave power based on the observed magnetic spectra and the crude conductivity model described above (Everett *et al.* (2003)). It is obvious that a correct estimate of the conductivity profile is critical for a correct prediction of the electric spectra. The error of the modeled electric spectra based on the crude conductivity model exceeds the error of the modeled electric spectra based on the modeled magnetic spectra and true conductivity profile by several dB. Thus, it seems more critical to have an accurate global conductivity model than improving the model of the geomagnetic spectra. The absolute error in dB between observed and modeled electric spectra (red dashed line) for all the 93 days of existing data is shown in Figure 10. The errors are consistently low for high frequencies throughout the period.

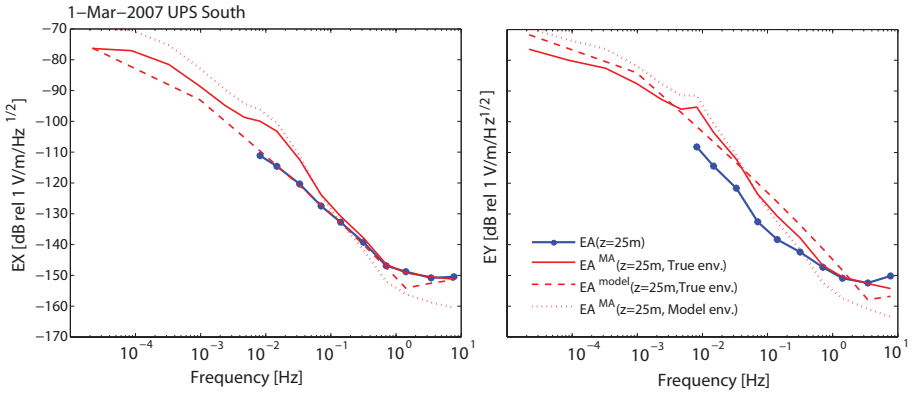

Figure 4.2: Observed and modeled electric spectra for the south system in Djupviken. The blue line corresponds to the observed spectra, the red line to the modeled spectra based on the observed magnetic spectra and true geology while the dashed red line corresponds to the modeled electric spectra based on the modeled magnetic spectra and true geology. The dotted red line corresponds to the modeled electric spectra based on the observed magnetic spectra and geology based on the global conductivity model.

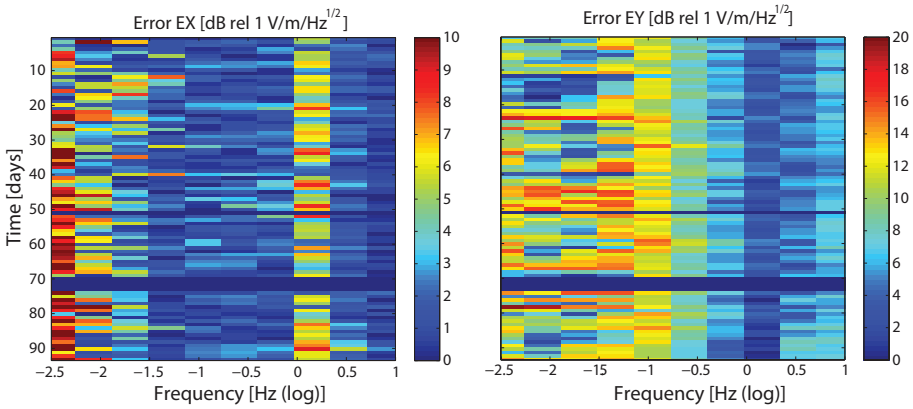

Figure 4.3: The absolute error in dB between observed and modeled electric spectra for all the 93 days of existing data.

5 Conclusions

The results of this work can be summarized as follows:

- A method has been developed to estimate the electromagnetic noise background at any given position at an arbitrary depth below the surface of the Earth.
- The method consists of the following three steps:
    1. Estimate the daily magnetic wave power amplitude at a given position.
    2. Relate the daily wave power amplitude to the geomagnetic spectrum up to a frequency of 10 Hz.
    3. Calculate the electric wave power spectrum at an arbitrary depth based on the theory of electromagnetic induction.
- The daily magnetic wave power amplitude from a semi-empirical model of geomagnetic variations is related to the geomagnetic spectrum from a found empirical relationship of the slope of the geomagnetic spectrum with geomagnetic activity.
- Comparison of the modeled electric noise with experimental measurements at a depth of 25 meters below the ocean surface in the Stockholm archipelago show good agreement.
- Preliminary results show that the model is more sensitive to uncertainties in the water conductivity than uncertainties in the spectral geomagnetic estimate.
- Further studies of the model are needed to validate the method and improve vital components in the method chain. Especially, further analysis of higher frequency data (sampled at 40 Hz) is necessary. Also, the reason behind the discrepancy between the daily wave powers derived from the CM4 model compared to observations needs to be investigated further.

Acknowledgements

We acknowledge the use of the CM4 model developed jointly between the magnetic groups at Goddard Space Flight Center (NASA/GSFC) and the Danish Space Research Institute. A special thanks to Nils Olsen for valuable help with the model. The results presented in this paper rely on data collected at magnetic observatories. We thank the national institutes that support them and INTERMAGNET for promoting high standards of magnetic observatory practice (www.intermagnet.org). We also acknowledge the use of magnetic activity indices derived from NCEDC data at Parkfield calculated by Martin Fullekrug from the University of Bath and the use of magnetic data from SGU. Geomagnetic activity indices used in this study have been retrieved from the Coordinated Data Analysis Web (CDAWeb).

Bibliography

Berdichevsky, M. N. & Zhdanov, M. S. 1984 *Advanced theory of deep geomagnetic sounding*, volume 19. Methods in geochemistry and geophysics, Elsevier Science.

Constable, C. G. & Constable, S. C. 2004 Satellite magnetic field measurements: applications in studying the deep earth. *In The State of the Planet: Frontiers and Challanges in Geophysics, American Geophysical Union*, **10.1029/150GM13**, 147–160.

Egbert, G. D., Eisel, M., Boyd, O. S. & Morrison, H. F. 2000 Dc trains and pc3s: Source effects in mid-latitude geomagnetic transfer functions. *Geophys. Res. Lett.*, **27**, 25–28.

Everett, M. E., Constable, S. & Constable, C. G. 2003 Effects of near-surface conductance on global satellite induction responses. *Geophys. J. Int.*, **153**, 277–286.

Laske, G. & Masters, G. 1997 A global digital map of sediment thickness. *EOS, Trans. AGU*, **78**, F483.

Mann, I. E., O'Brien, T. P. & Milling, D. K. 2004 Correlations between ulf wave power, solar wind speed, and relativistic electron flux in the magnetosphere: solar cycle dependece. *J. of Atmosph. and Sol.-Terr. Phys.*, **66**, 187–198.

Ponomarenko, P. V., Fraser, B. J., Menk, F. W., Ables, S. T. & Morris, R. J. 2002 Cusp-latitude pc3 spectra: band-limited and power-law components. *Ann. Geophys.*, **20**, 1539–1551.

Sabaka, T. J., Olsen, N. & Purucker, M. E. 2004 Extending comprehensive models of the earth's magnetic field with ørsted and champ data. *Geophys. J. Int*, **159**, 521–547.

Tyler, R. H., Mysak, L. A. & Oberhuber, J. M. 1997 Electromagnetic fields generated by a three dimensional global ocean circulation. *J. Geophys. Res.*, **102**, 5531–5551.

Vallee, M. A., Newitt, L., Dumont, R. & Keating, P. 2005 Correlation between areomagnetic data rejection and geomagnetic indices. *Geophysics*, **70**, J33–J38.